Characterizing Land–Atmosphere Coupling and the Implications for Subsurface Thermodynamics

MARC STIEGLITZ

School of Civil and Environmental Engineering, and School of Earth and Atmospheric Sciences, Georgia Institute of Technology, Atlanta, Georgia

JASON E. SMERDON

Lamont-Doherty Earth Observatory, Columbia University, Palisades, New York

(Manuscript received 7 December 2005, in final form 4 May 2006)

ABSTRACT

The objective of this work is to develop a Simple Land-Interface Model (SLIM) that captures the seasonal and interannual behavior of land–atmosphere coupling, as well as the subsequent subsurface temperature evolution. The model employs the one-dimensional thermal diffusion equation driven by a surface flux boundary condition. While the underlying physics is straightforward, the SLIM framework allows a qualitative understanding of the first-order controls that govern the seasonal coupling between the land and atmosphere by implicitly representing the dominant processes at the land surface. The model is used to perform a suite of experiments that demonstrate how changes in surface air temperature and coupling conditions control subsurface temperature evolution. The work presented here suggests that a collective approach employing both complex and simple models, when joined with analyses of observational data, has the potential to increase understanding of land–atmosphere coupling and the subsequent evolution of subsurface temperatures.

1. Introduction

In efforts to describe the dynamics at the land–atmosphere boundary, a principal focus of the climate community has been the development and validation of land surface models for controlled experiments and forecasting. This endeavor has largely concentrated on modeling schemes that seek to incorporate a robust representation of processes operating at the land–atmosphere boundary in order to realistically capture the exchange of energy, mass, and momentum across the interface. Such efforts have generated a host of complex models, a generic term used here to represent those schemes that include explicit representations of factors such as snow and permafrost dynamics, biophysical exchanges associated with vegetation, topographic control over surface hydrology, etc. (e.g., Henderson-Sellers et al. 1993, 1995; Dickenson et al. 2002; Koster et al. 2000; Stieglitz et al. 1997). The utility of such efforts is widely recognized, with many applications that include integration into GCMs and weather forecasting across many spatial scales (e.g., Dickenson and Henderson-Sellers 1988; Koster and Suarez 1992; Garratt 1993; Betts et al. 1996; Sellers et al. 1997; Koster et al. 2000; Dai et al. 2003; Pitman 2003).

While development of complex models has lead to great successes, there are other approaches to understanding the dynamics of land–atmosphere coupling that have yet to be widely investigated. One such approach uses modeling frameworks that implicitly represent the first-order controls operating on and beneath the land surface by using simple governing equations that depend on very few parameters. The objective of such an approach derives from the need to provide a more qualitative and general understanding of land–atmosphere coupling across a diverse range of climates and environments. Such understanding can often be elusive when using complex models that are designed to represent the full suite of controlling processes and rely on highly specific data to validate model formulations and calibrate parameters—data often not widely avail-

Corresponding author address: Marc Stieglitz, School of Civil and Environmental Engineering, Georgia Institute of Technology, 790 Atlantic Dr. NW, Atlanta, GA 30332-0355.
E-mail: marc.stieglitz@ce.gatech.edu

DOI: 10.1175/JCLI3982.1

able. By contrast, Simple Land-Interface Models (SLIMs), if properly designed, can more fully exploit existing meteorological data and depend on only a few parameters, making these models widely applicable and easy to interpret. The objective of these modeling frameworks is to establish a balance between interpretability and accurate characterizations of the gross features of land–atmosphere dynamics. The proposal of such a representation is the principal goal of this manuscript.

The suggestion that simple formulations can capture the behavior of coupling at the land–atmosphere boundary is not without precedent. Several areas of investigation have already demonstrated a range of simpler frameworks that describe phenomena tied to the coupling of the land and atmosphere. Analyses of borehole temperature profiles as indicators of historical surface temperature change typically assume that the subsurface is conductive and that long-term changes in ground surface temperatures (GSTs), that is, changes on decades, centuries, or longer, are closely coupled to changes in surface air temperature (SAT) at equivalent periods. Comparisons between the temporal and spatial variation in GST reconstructions and direct measurements of SAT have widely validated these assumptions (e.g., Chisholm and Chapman 1992; Beltrami et al. 1992; Bodri and Cermak 1995, 1997; Gosnold et al. 1997; Harris and Gosnold 1999; Huang et al. 2000; Harris and Chapman 2001; Roy et al. 2002; Pollack et al. 2003; Pollack and Smerdon 2004). At daily, seasonal, and annual time scales, however, thermal coupling between the air and subsurface can be highly variable, depending on meteorological conditions (e.g., Putnam and Chapman 1996; Zhang et al. 2001; Schmidt et al. 2001; Beltrami 2001; Baker and Baker 2002; Stieglitz et al. 2003; Lin et al. 2003; Beltrami and Kellman 2003; Smerdon et al. 2003, 2004; Bartlett et al. 2004; Grundstein et al. 2005; Hu and Feng 2005). Nevertheless, several investigations have shown that differences between air and subsurface temperatures at these short time scales can be captured with simple conductive models that couple the atmosphere and ground with time-varying boundary layers that change according to meteorological conditions (Bartlett et al. 2004; Pollack et al. 2005; Bartlett et al. 2005) or with statistical models that use seasonal meteorological conditions as predictors of air and ground temperature differences (Smerdon et al. 2006).

We develop a simple modeling framework that allows investigations into land–atmosphere coupling and the subsequent impacts on subsurface thermodynamics across a broad range of climates and environments. We perform a qualitative analysis that employs a SLIM scheme to increase our understanding of the seasonal controls that govern subsurface temperature evolution. Our focus is on seasonal characterizations of coupling between the land and atmosphere at what could be considered a point location. The governing equations of our model are given in section 2. Experimental design is described in section 3, and in section 4 we display and discuss the simulation results. Finally, section 5 presents observational and simulated data to corroborate the general characteristics of the simulations with real-world observations.

2. Model formulation

The application of the diffusion equation to describe heat transport beneath the earth's surface is a well-established concept (e.g., Carslaw and Jaeger 1959; Campbell 1977; Gildyal and Tripathi 1987; Hillel 1998; Geiger et al. 2003). Such applications typically employ the one-dimensional form of the equation, assuming a homogeneous subsurface:

$$\frac{\partial T(z, t)}{\partial t} = D \frac{\partial^2 T(z, t)}{\partial z^2}, \tag{1}$$

where T is temperature, z is depth, t is time, and D is the thermal diffusivity defined as the ratio between the thermal conductivity and the volumetric heat capacity.

We calculate steady-state and transient solutions to Eq. (1) assuming a homogeneous subsurface, a time-varying flux boundary condition at the land surface, and a zero-flux boundary condition at the bottom of the deepest modeled layer. The land surface boundary condition is used to represent the temporal evolution of the coupling between the land and atmosphere and is written as

$$\left.\frac{\partial T}{\partial t}\right|_{z=0,t} = c(t)[T_{\text{air}}(t) - T(0, t)], \tag{2}$$

where T_{air} is the SAT, $T(0, t)$ is the GST, and $c(t)$ is the coupling coefficient, a factor that theoretically ranges from 0 (no coupling) to infinity (perfect coupling). The coupling can also depend on the thermal conductivity of the subsurface, but here we consider constant subsurface thermophyiscal properties and therefore coupling only changes according to $c(t)$ [1/time].

The suggestion that much of the coupling dynamics at the land–atmosphere boundary can be implicitly represented in terms of a single coupling function, $c(t)$, is the principal postulate of this manuscript. Within the proposed modeling framework, the temporal character of $c(t)$ represents the variable coupling between SAT and GST and is determined from observational data. Thus, the cumulative effects of the processes operating at the land–atmosphere interface are subsumed into a

single term that determines the overall strength of coupling between the air and ground at any given time scale. Hence, the SLIM representation that we employ is the one-dimensional diffusion equation coupled to SAT by the flux condition [Eqs. (1) and (2)].

3. Experimental design

There are two basic steps in our experimental approach. A baseline simulation is conducted (hereafter referred to as the "spinup simulation") by running SLIM until the subsurface reaches thermal equilibrium, a condition defined here as when the average annual temperature–depth profile is static. Equilibrium conditions from the end of the spinup simulation are used to initialize subsurface temperatures, a continuous change is then imposed in the surface forcing conditions (i.e., changes in the SAT, the coupling coefficient, or both). All simulations employ a zero-flux boundary condition at 20-m depth. This depth is well below the damping depth of the annual signal, but shallow enough to allow for solutions to converge within reasonable computation times. Constant thermophysical properties are assumed in the subsurface and we assign a thermal diffusivity of 30 m^2 yr^{-1}, a value within the typical range of diffusivity for soils and common crustal rocks (e.g., Hillel 1998; Carslaw and Jaeger 1959). In the following sections we describe our choices for the functional forms of the spinup SAT and coupling coefficient, as well as the chosen experimental changes to each of these functions.

a. *Spinup temperature and flux boundary condition functions*

Our objective is to gain first-order insight into the evolution of subsurface temperatures and the seasonal coupling between SAT and GST. The absolute magnitudes of subsurface temperature changes are not of concern, and each experiment is formulated in terms of percent changes relative to the spinup simulation. We employ a sinusoidal SAT function of unit amplitude and annual period to drive the spinup simulation. SAT is the principal forcing in the model and is coupled to the subsurface via the coupling coefficient [Eq. (2)]. The spinup SAT is plotted in Fig. 1.

SLIM also requires a representation of the coupling function, $c(t)$. To provide a qualitative understanding of the role that the coupling function plays within the SLIM framework, we perform a set of simulations using constant $c(t)$ functions; the chosen values are 10, 8, 6, 4, and 2 yr^{-1}. For each of these values the model is forced with SAT sinusoids, having periods that range from 0.04 to 10 yr. The GST is calculated for each SAT sinusoid, which is then used to calculate the ratio between the GST and SAT amplitudes. We refer to the attenuation of the GST signal as the difference between 100% and the percent ratio of the GST and SAT amplitudes.

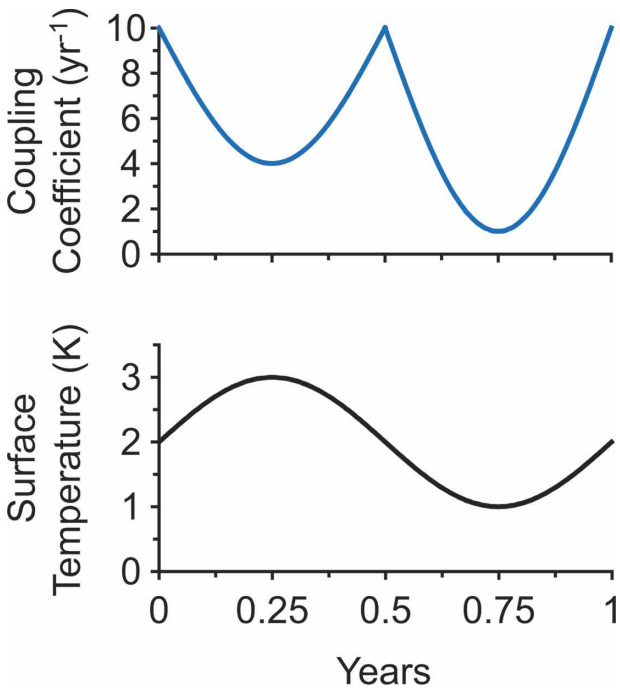

FIG. 1. Representation of (top) the coupling coefficient and (bottom) the surface temperature used in the spinup simulations. The spinup simulations were for 80 yr and used to initialize the subsequent 6-yr experiments that involved changes to the coupling coefficient and surface temperature functions shown here.

Figure 2 plots the GST attenuation over a range of frequencies. The two most prominent features depicted in Fig. 2 are 1) increasing signal attenuation with decreasing values of $c(t)$, and 2) increasing signal attenuation with increasing SAT frequency. Regarding the first feature, GST with a period of 1 yr is attenuated by 15% and 3%, relative to SAT, for a $c(t)$ equal to 2 and 10, respectively. The frequency dependence of the second feature is tied to the thermophysical properties of the subsurface that determine the rate at which the ground can respond to changes in SAT. Given specific thermophysical properties (here we have assumed D = 30 m^2 yr^{-1}), the ground fails to track the full magnitude of high-frequency SAT fluctuations because it cannot respond fast enough; hence, the behavior demonstrated in Fig. 2.

Land–atmosphere coupling is not constant over the course of a year and therefore a temporally varying form of $c(t)$ must be determined to perform SLIM simulations that are representative of the land–atmosphere system. The seasonal behavior of $c(t)$ is governed by numerous factors such as snow insulation,

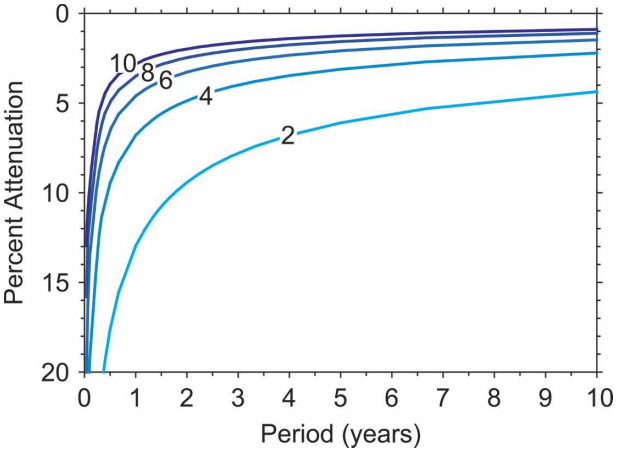

FIG. 2. Dependence of GST attenuation on the value of the coupling coefficient and the frequency of SAT oscillations. GST attenuation is defined as the difference between 100% and the percent ratio of the GST and SAT amplitudes. Each curve in the plot represents responses for different constant values of the coupling coefficient. For each curve the GST attenuation was investigated over a range of frequencies with periods from 0.4 to 10 yr.

vegetative insulation, freeze–thaw processes, vapor transport in soils, evapotranspiration, and wind. These factors act to influence the coupling between the air and ground in complex ways (e.g., Lin et al. 2003; Smerdon et al. 2004, 2006; Goodrich 1982; Kane et al. 2001; Sokratov and Barry 2002; Stieglitz et al. 2001, 2003). Nevertheless, there are general patterns to the relationships between air and ground temperatures that depend on only several dominant processes. To elucidate the seasonal nature of the coupling we consider six sites, each vegetated and either with or without snow cover in winter. We discuss these sites in detail in section 3c and in the appendix, but here we summarize the temporal behavior of land–atmosphere coupling at the sites as a justification for the functional form of $c(t)$ that we adopt. Two principal differences between air and ground temperatures arise at the six sites: 1) in the summer the ground is cooler than the air because it is insulated by vegetative processes; and 2) in the winter the ground is warmer than the air due to the insulating effects of snow cover. Given this seasonal behavior, we choose the functional form of $c(t)$ plotted in Fig. 1. The chosen coupling function reaches two minimums, one in midsummer and one in midwinter, and is representative of the gross features of coupling observed at the six sites.

b. Choosing the range of changes in spinup temperatures

We analyze data from North America to estimate regional variability in SAT and coupling coefficients. SAT variability is estimated from the nine regional divisions of the contiguous United States as defined by the National Climatic Data Center (NCDC): northwest, west-north central, east-north central, central, Northeast, West, Southwest, South, and southeast regions (see the NCDC Web site for detailed information on these divisions: http://www.ncdc.noaa.gov/oa/ncdc.html). The data for these nine regions are from the U. S. Historical Climatology Network (Karl et al. 1990) and provide mean temperatures for summer (June–August) and winter (December–February) during the period 1896–2004. From these data we determine variability in the SAT summer maxima and winter minima. The percent variability of seasonal SAT amplitudes in each of the nine regions are computed using the following steps: 1) the long-term summer and winter mean air temperatures are computed from 1896 to 2004, 2) the associated standard deviations for the summer and winter means are calculated, 3) half the difference between the seasonal means in step 1 is computed to yield the magnitude of the SAT amplitude within each region, and 4) the percent deviation of summer and winter amplitudes are determined by dividing twice the seasonal standard deviation (includes 95% of the amplitude deviations) by the magnitude of seasonal SAT amplitudes from step 3. Across the continental United States, these amplitudes ranged from 4.27 to 7.02 K. The standard deviation of summer and winter means ranged from 0.5–1.0 and 1.3–2.0 K, respectively. Thus, we estimate the corresponding ranges of seasonal amplitude variability in the summer and winter seasons to be 11.7%–16.2% and 24.5%–34.8%, respectively. These statistics are summarized in Table 1. Based on these estimates, we explore changes in summer SAT amplitudes of ±15% and in winter SAT amplitudes of ±30%, values close to the mean of all nine regions. These changes are represented schematically in Fig. 3.

c. Choosing spinup coupling coefficients

It is more difficult to estimate ranges of coupling coefficient variability, as no general theory has been developed to characterize it. It is possible, however, to achieve a preliminary estimate of seasonal coupling behavior using empirical comparisons of air and ground temperatures. Here we consider the above-mentioned six sites, which span a diverse range of climates and environments: Fargo, North Dakota (46°54′N, 96°48′W); Cape Henlopen State Park, Delaware (38°46.4′N, 75°5.7′W); Cape Hatteras National Seashore, North Carolina (35°15.2′N, 75°32.0′W); Campbell River, British Columbia (49°52.14′N, 125°20.12′W); Sylvania Wilderness, Michigan (46°14.52′N, 89°20.86′W); and Bondville, Illinois (40°0.37′N, 88°17.51′W). Table 2

TABLE 1. Summary of regional statistics for amplitude variability in the contiguous United States.

Region	Season	Mean (°C)	Std dev (°C)	Amplitude (°C)	% Range of amplitude
Northwest	Summer	17.51	0.73	9.20	15.92
	Winter	−0.89	1.53		33.25
West-north central	Summer	19.08	0.95	6.50	14.59
	Winter	−6.93	2.01		30.96
East-north central	Summer	19.85	0.95	7.02	13.50
	Winter	−8.22	1.98		28.26
Central	Summer	23.23	0.85	5.77	14.79
	Winter	0.17	1.72		29.79
Northeast	Summer	19.60	0.69	5.98	11.51
	Winter	−4.33	1.60		26.80
West	Summer	21.81	0.71	4.38	16.17
	Winter	4.32	1.27		29.08
Southwest	Summer	21.65	0.69	5.22	13.16
	Winter	0.79	1.28		24.46
South	Summer	26.71	0.71	5.00	14.19
	Winter	6.72	1.29		25.85
Southeast	Summer	25.52	0.50	4.27	11.72
	Winter	8.43	1.49		34.76

summarizes the climates and environments at each of these sites, which include maritime and intercontinental climates in forest, grassland, gassy dune, and cropland settings.

Smerdon et al. (2004) have analyzed the Fargo, Cape Henlopen, and Cape Hatteras datasets to compare the amplitudes of annual SAT and GST signals. Here we analyze the three additional sites using data obtained from the Ameriflux database (see online at http://public.ornl.gov/ameriflux/). The annual SAT and GST signals for the Campbell River, Sylvania Wilderness and Bondville sites are shown in Fig. 4 [see Smerdon et al. (2004) for a similar figure showing the Fargo, Cape Henlopen, and Cape Hatteras results]. Further descriptions of the sites and our analysis are given in the appendix. At all sites the annual GST signal was attenuated relative to SAT. For instance, large forest canopies at the Campbell River and Sylvania Wilderness sites caused significant summer decoupling between SAT and GST. Snow cover plays a significant role in decoupling the air and ground at the Sylvania Wilderness and Bondville sites, the two midlatitude intercontinental sites, and is similar to the results found at Fargo (Smerdon et al. 2003).

Collectively, the six sites represent an attempt to quantify the magnitude of effects from different forms of seasonal decoupling; summer and winter decoupling ranged from approximately 0% to 25% and from 0% to 40%, respectively. These ranges reflect spatial variability, and are likely larger than the temporal variability at any given site. With this in mind, we select a spinup coupling coefficient with minimum summer and winter values of 4 and 1 yr^{-1}, respectively, yielding summer and winter GST attenuations of approximately 7% and 23%, respectively. Summer coupling coefficient minimums of 10 and 3 yr^{-1} are also investigated, representing high and low summer coupling scenarios that yield GST attenuations of 3% and 10%, respectively. Winter coupling coefficient minimums of 3 and 0 yr^{-1} are investigated, representing high and low winter coupling scenarios that yield GST attenuations of 10% and 32%, respectively. This set of coupling coefficient changes, when combined with the set of SAT changes described in the previous section, define a total of nine experiments. Figure 3 displays each of the experimental changes, and Table 3 gives the maximum and minimum values of the SAT and coupling coefficients for the spinup and the nine experiments.

4. Experimental results

a. Spinup simulation

Figure 5 displays the last 6 yr of the spinup simulation and demonstrates the characteristic features of diffusing temperature signals. Seasonal temperatures penetrate into the subsurface causing an alternating warming and cooling within the first several meters of the subsurface. These seasonal temperature lobes are attenuated and phase lagged with depth and the annual oscillations are almost fully attenuated by 10 m, consistent with theory (see Carslaw and Jaeger 1959).

The spinup simulations also demonstrate the effects of the changing coupling coefficient. GST is attenuated in both the summer and winter seasons due to reduced

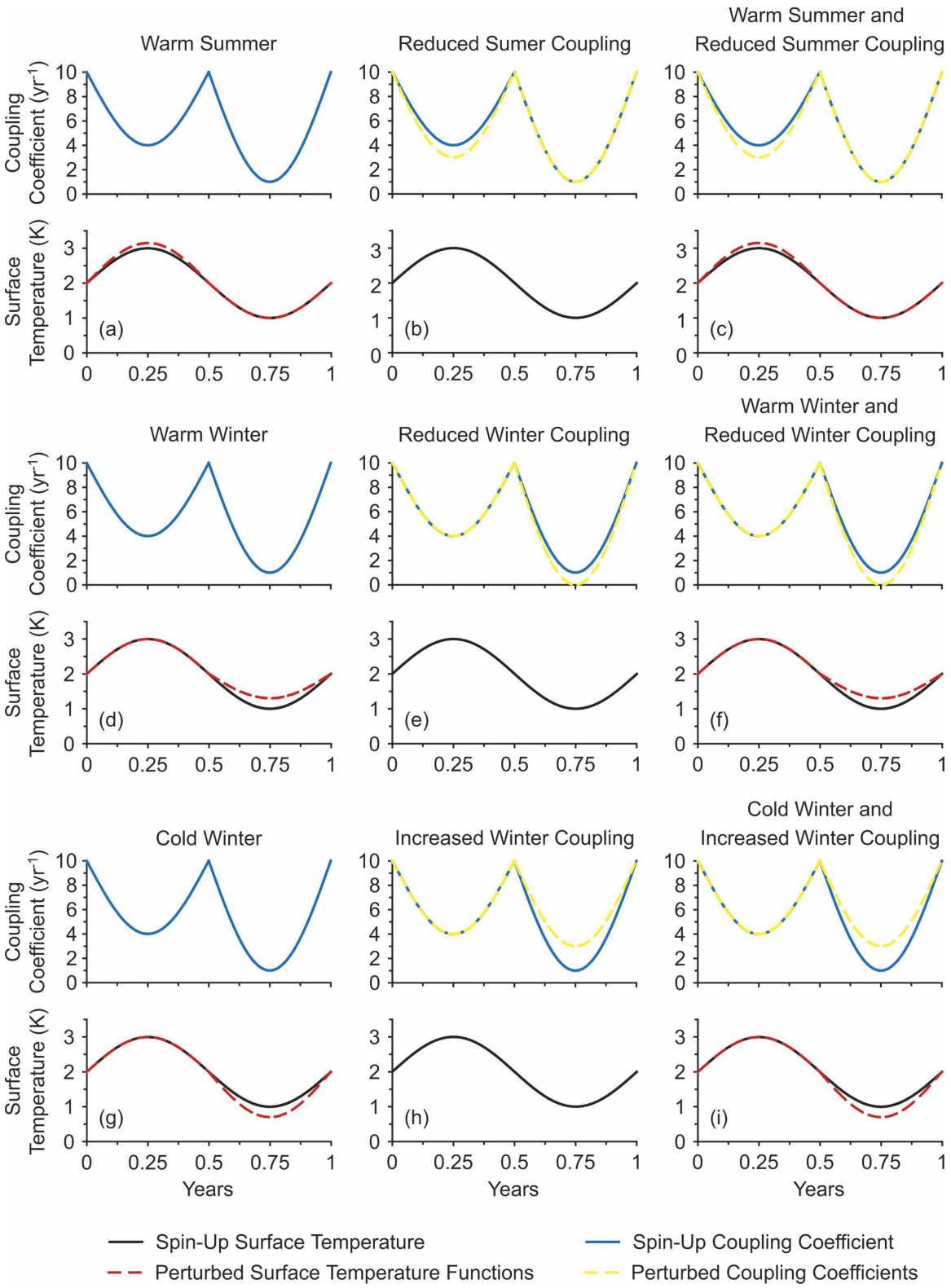

FIG. 3. Graphical representation of the nine experiments discussed in section 5. Each of the plots shows the experimental changes in surface temperature and coupling coefficients relative to the spinup conditions. These perturbations were imposed for 6 yr after 80 yr of the spinup simulation. The lettering of each panel corresponds to the lettered descriptions in sections 5b, 5c, and 5d.

TABLE 2. Summary of the six sites used to estimate coupling coefficient variability.

Site	Climate	Biome	Percent of summer decoupling	Percent of winter decoupling
Fargo, ND	Midlatitude, intercontinental	Grassland	~0%	~23%
Cape Henlopen, DE	Maritime	Dune	~8%	~0%
Cape Hatteras, NC	Maritime	Dune	~8%	~0%
Bondville, IL	Midlatitude, intercontinental	Cropland	~0%	~15%
Sylvania Wilderness, MI	Midlatitude, intercontinental	Mixed forest	~18%	~40%
Campbell River, BC, Canada	Maritime	Evergreen forest	~25%	~6%

coupling during those seasons. The effects are illustrated in Fig. 6, showing the SAT, GST, and 1-m time series model outputs. The peak summer GST is 2.93 K, compared to the summer SAT maximum of 3 K. Similarly, the minimum winter GST is warmer than the SAT, with values of 1.23 and 1 K, respectively. These seasonal differences are also reflected in the mean annual GST, equal to 2.04 K; the mean SAT is 2 K. This increased GST mean value is indicative of the asymmetric behavior of the warming and cooling of the subsurface caused by the seasonal differences in the coupling coefficient.

b. *Warmer summers and increased summer decoupling*

The first suite of experiments is focused on summer effects. The three simulated scenarios are A—6 yr of warm summers in which the peak SAT increases from the spinup value of 3 to 3.15 K, B—6 yr of increased summer decoupling in which the minimum summer coupling coefficient is reduced from the spinup value of 4 to 3 yr^{-1}, and C—6 yr of combined warm summers (scenario A) and increased decoupling (scenario B). Figure 7 is a schematic illustrating the implementation of the above experimental scenarios. After the 80-yr spinup simulation, the SAT and coupling coefficient functions are changed according to each scenario and the model is run for an additional 6 yr. The last 6 yr of the spinup simulation are shown on the left-hand side of the figure, along with the SAT and coupling coefficient functions used to drive the spinup run. The three right panels in Fig. 7 are the 6 yr of simulated temperatures after the changes have been imposed. The experimental approach represented in Fig. 7 is used in all of the experiments that follow.

The 6-yr subsurface transient responses for scenarios A–C are displayed in Fig. 8. Six warm summers in scenario A yield progressively deeper intrusions of the summer temperature lobe and a small warming of winter ground temperatures. These changes slowly propagate to depth and warm the subsurface to 20 m during the fifth year. Under conditions of increased summer decoupling in scenario B, midsummer ground temperatures are colder than those in scenario A and spinup simulation. There is, however, no significant deep intrusion of the summer temperature lobe. The winter lobe is colder in the middle of winter, and diffuses to greater depths than either the warm summer or spinup simulations. Interestingly, the cooling due to reduced summer coupling impacts not just the evolution of summer temperatures, but the winter temperatures as well. In fact, winter changes are progressively more pronounced with depth than the summer changes. This effect likely arises because cold early-winter temperatures would normally "compete" with the deep upward flux of heat stored from the previous summer. The increased summer decoupling of scenario B, however, reduces summer ground temperatures at the surface and at depth. Cold winter temperatures therefore penetrate more easily without encountering deep upward fluxes of heat from the previous summer.

Scenario C combines warmer summers with reduced summer coupling. The results are similar to those of only the warm summer scenario A. This simulation implies that within the ranges of imposed changes, increases in summer temperatures more than offset the impact of reduced coupling. One important consequence of the effect may be in regions where winter ground temperatures are very near freezing. Scenarios A–C suggest that in some regions, summer coupling may have the potential to increase or decrease the likelihood of winter ground freezing under otherwise very similar winter conditions.

c. *Warmer winters and increased winter decoupling*

The second suite of experiments is focused on winter effects. The three simulation scenarios are as follows: D—6 yr of warm winters in which the minimum winter SAT increases from the spinup value of 1 to 1.3 K, E—6 yr of reduced winter coupling in which the minimum winter coupling coefficient is reduced from the spinup value of 1 to 0 yr^{-1}, and F—6 yr of combined warm

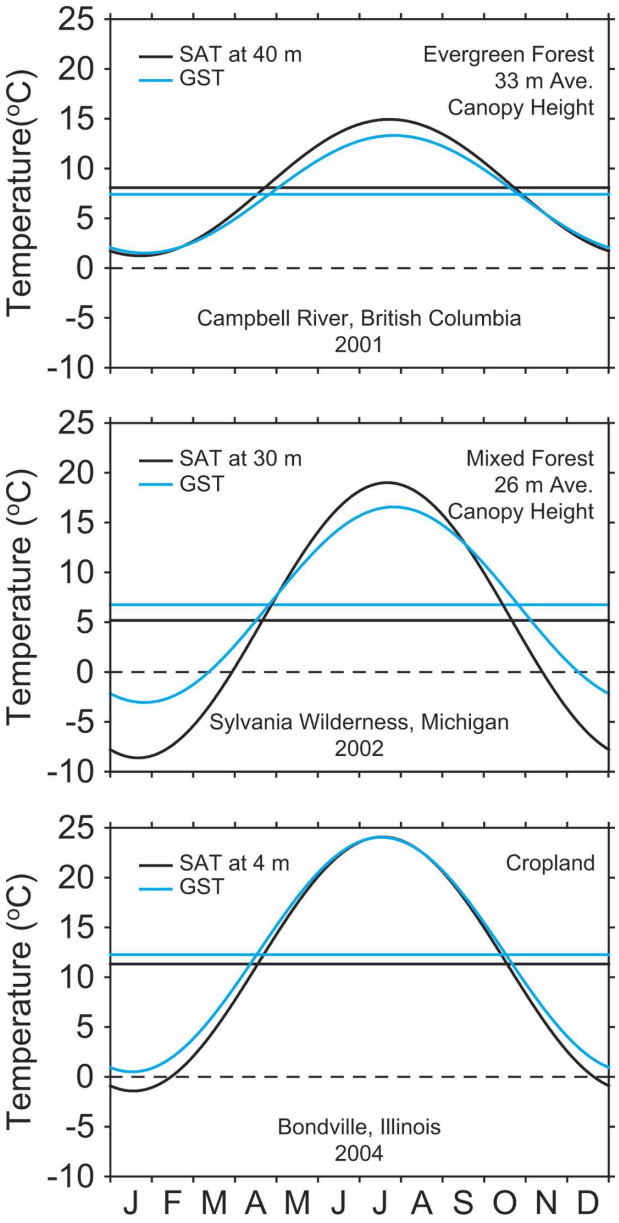

FIG. 4. Annual SAT (black) and GST (blue) signals from observational sites at (top) Campbell River, BC, Canada; (middle) Sylvania Wilderness, MI; and (bottom) Bondville, IL. SAT signals have been referenced to their respective means and GST signals have been referenced to approximate ground surface means using the closest near-surface measurement in each dataset. The ordinate in each panel spans different ranges, but each linear scaling is equivalent.

winters (scenario D) and reduced winter coupling (scenario E).

The 6-yr transient responses of the subsurface to scenarios D–F are displayed in Fig. 9. Under conditions of warmer winters in scenario D, temperatures in the shallow subsurface are not as cold as the spinup simulation.

TABLE 3. Summary of maximum and minimum values of the driving conditions for the spinup and experimental simulations.

Driving conditions	Spinup	Max increase	Max decrease
Peak summer temperature	3 K	3.15 K	2.85 K
Peak winter temperature	1 K	1.3 K	0.7 K
Peak summer $c(t)$	4 yr^{-1}	10 yr^{-1}	3 yr^{-1}
Peak winter $c(t)$	1 yr^{-1}	3 yr^{-1}	0 yr^{-1}

The temperature gradient during the winter season is also reduced, while the flattened isotherms in the near surface have broadened and extended in time. The summer temperature lobes also get warmer and reach deeper into the subsurface, once again demonstrating the potential for single-season changes to have interseasonal consequences in subsurface temperature responses.

For scenario E, in which there is greater winter decoupling, the near-surface winter isotherms are separated into two distinct asymmetric bulges, a small shallow cold bulge in early winter and a larger cold bulge in late winter. Similar features have been noted in observations of arctic subsurface temperatures (H. Bader, Department of Natural Resources, Alaska, 2004, personal communication). We interpret this for real-world conditions as follows: air and ground temperatures fall together in early winter when snow depth is relatively shallow and the coupling between SAT and GST is still strong. As snow depth nears its maximum in midwinter, SAT–GST coupling is near its minimum. This allows upward fluxes of heat from the previous summer to warm the near-surface in midwinter, distorting the normally symmetric winter ground temperature lobe. Finally, as the snowpack depth is reduced in late winter due to densification and melt, SAT–GST coupling is reestablished, leading to penetration of cold SATs and the subsequent development of a pronounced second winter temperature bulge in the subsurface. For the combination of warm winters and increased snowfall in scenario F, the front side of the winter temperature lobe is further eroded and separated into the distinct two-bulge feature.

The results of scenarios D–F have particular relevance at high latitudes where the magnitude and spatial extent of air and subsurface warming has been well documented (e.g., Lachenbruch and Marshall 1986; Oberman and Mazhitova 2001; Osterkamp and Romanovsky 1994, 1999; Pavlov 1994; Zhang et al. 1997; Foster 1989; Foster et al. 1992; Stone et al. 2002; Chapman and Walsh 1993; Houghton et al. 2001; Overpeck and al. 1997; Serreze et al. 2000). In particular, they yield insights into an apparent paradox; the paradox

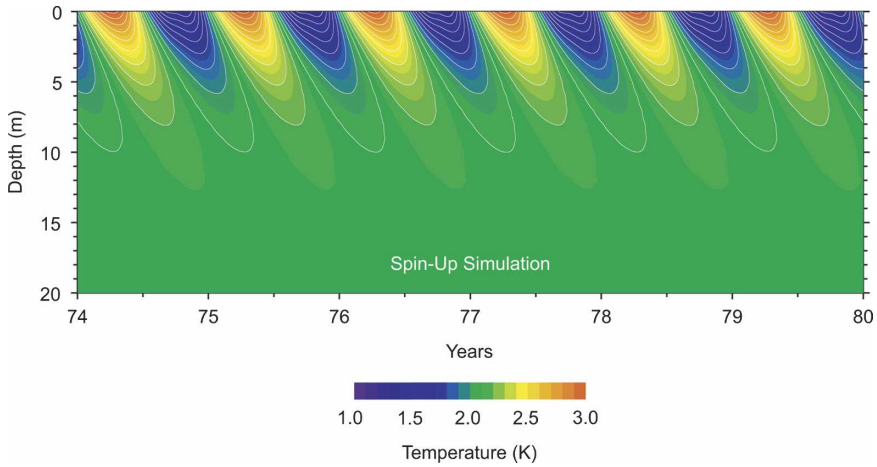

FIG. 5. Last 6 yr of the spinup simulation showing the diffusion of the oscillating surface signal in to the subsurface. The character of the winter lobe is different than the summer lobe due to the asymmetry of the coupling coefficient shown in Fig. 1. At about 10 m the annual signal is damped out and constant temperatures persist below that depth.

being that while atmospheric warming in the arctic has predominantly been a winter and winter/spring phenomenon (McBean et al. 2005), the lengthening of thawed ground conditions has occurred in both the fall and spring (Smith et al. 2004). Figure 9 demonstrates how this seemingly unrelated cause and effect might be so. As noted earlier, warm winters (air temperatures),

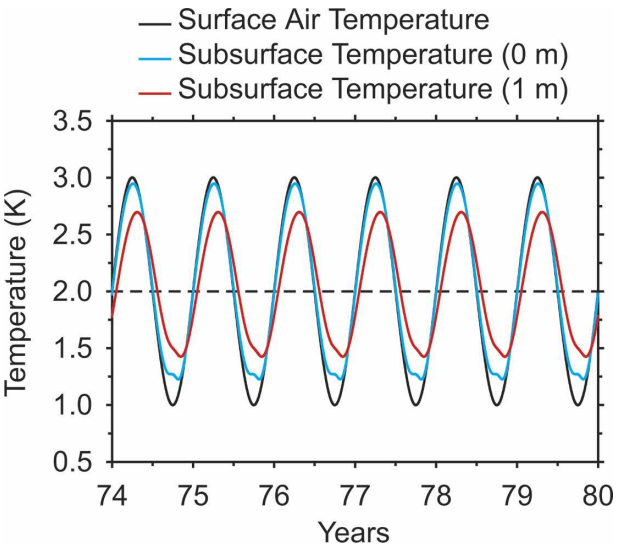

FIG. 6. Temperature time series plots of the SAT, the GST, and the 1-m subsurface temperature as computed from SLIM in the last 6 yr of the spinup simulation. The dashed line in the figure is the mean of the SAT. Decoupling between SAT and GST due to changes in the coupling coefficient is evident in both the summer and winter, although the winter decoupling is much larger. Changes in GST, relative to SAT, are communicated to depth, as shown in the 1-m output.

especially those with a deeper-than-normal snowpack (reduced coupling), indirectly impact the evolution of ground temperatures in the following winter. After a few years of winter warming or less than normal winter coupling there is a compression of the winter lobes and a lateral expansion and deeper penetration of the summer signal. This intensified summer signal, achieved without an explicit warming of the summer, is then quite effective at keeping early winter ground temperatures warm. Nevertheless, while this subsurface warming in summer is sufficient to impact the evolution of subsurface temperatures in early and midwinter (note the double bulge in Fig. 9), its impact is much reduced by late winter. The impact of warmer than normal winter and spring air temperatures therefore has an immediate impact on the time of the spring thaw, but also a delayed impact on ground temperatures in the following fall.

d. Cold winters and increased winter coupling

The third suite of experiments is again focused on winter effects. The three scenarios are as follows: G—6 yr of cold winters in which the minimum winter SAT decreases from the spinup value of 1 to 0.7 K, H—6 yr of increased winter coupling in which the minimum winter coupling coefficient is increased from the spinup value of 1 to 3 yr^{-1}, and I—6 yr of combined cold winters (scenario G) and increased winter coupling (scenario H).

The 6-yr transient responses of the subsurface to scenarios G–I are displayed in Fig. 10, and demonstrate that all three scenarios generate colder winter temperature lobes. Both the cold winter and reduced snowfall

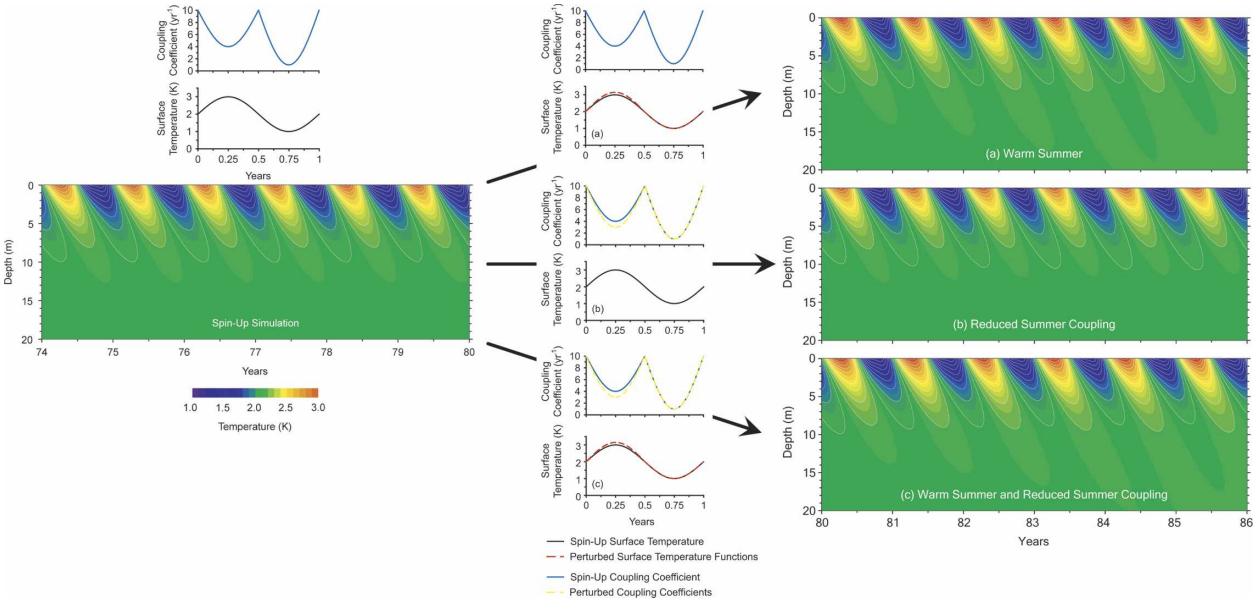

FIG. 7. Schematic illustration of how the simulation experiments are implemented using scenarios A–C. (left) The spinup forcing functions and the subsurface temperature field in the last 6 yr of the spinup simulation. The temperature profile at the end of the 80-yr spinup simulation is then used to initialize the subsurface at the beginning of 6-yr experiments. These experiments impose changes to the spinup SAT and coupling coefficient functions. (middle) Three examples of changes to the spinup functions are shown. (right) The 6 yr of subsurface temperature responses are shown for each experimental change.

experiments lead to colder winter subsurface temperatures that diffuse to deeper depths, phase shift with time, and spread throughout the profile. The cold winter plus reduced snowfall scenario (scenario I) reflects a combination of the two above scenarios (scenarios G and H).

Scenarios G–I highlight the different means by which winter conditions reduce the impact of upward fluxes from summer temperatures. In scenario G, winter temperatures are colder than normal and the subsurface is rapidly cooled. In this scenario, subsurface heat stored from the previous summer is not a major factor in driving midwinter temperatures. In scenario H, as midwinter coupling is increased the subsurface is no longer insulated from midwinter SAT, and the subsurface is rapidly cooled. As in scenario G, subsurface heat stored from the previous summer is not a major factor in driving midwinter temperatures. These dynamics of scenarios G and H are amplified in scenario I.

5. Corroborating support for SLIM

Validation or corroboration of a model's performance takes many forms. We conduct a qualitative assessment of SLIM by visually assessing the authenticity of structures and patterns that emerge from the model simulations. Such an assessment is consistent with the goal of this work, which is to gain a first-order understanding of the dynamics that govern the seasonal evolution of subsurface temperatures.

We first examine year-to-year variability in coupling characteristics using subsurface temperature observations taken at Fargo (see section 3c and in the appendix; Fig. 11). Meteorological conditions are also displayed, showing daily SAT and snow depth. The SAT in the winter of 1982–83 was warmer than that in 1983–84, yet the subsurface was cooled to a greater depth in 1982–83. The explanation for this is that snow depth was considerably less in 1982–83, which effectively increased SAT–GST coupling in that winter relative to 1983–84. Additionally, the SAT in the winter of 1981–82 was colder than either of the following 2 yr, but it was also a winter of extensive snow cover. The effect of these two conditions on subsurface temperatures in 1981–82 was to cancel each other and maintain temperatures that were about as cold as 1982–83 and slightly colder than 1983–84. Although quite qualitative, the behavior of the subsurface temperature evolution observed at Fargo is consistent with the simulations that we have performed, both in its respective responses to meteorological conditions and in the overall evolution of subsurface temperatures.

We now compare observed and simulated subsurface temperatures at Cape Hatteras (see section 3c and in

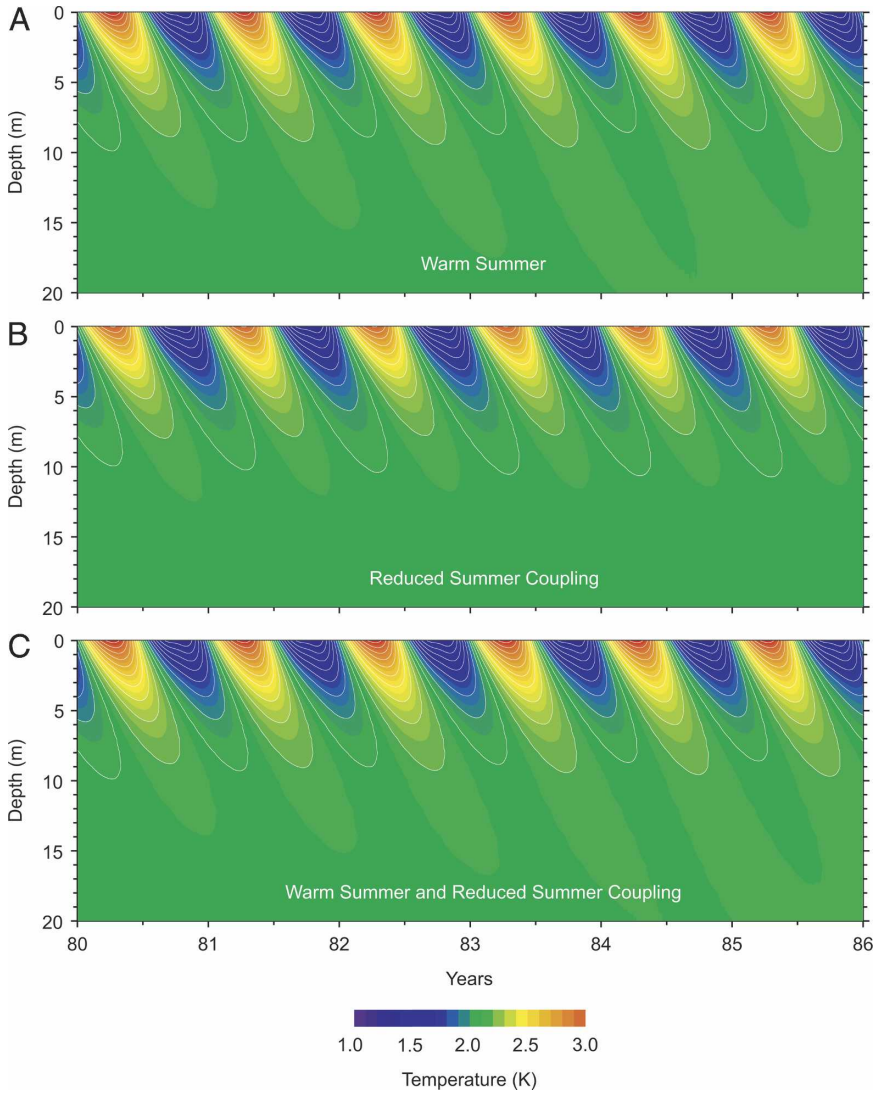

FIG. 8. Results from 6 yr of simulation after perturbations were imposed from the spinup conditions. This ensemble of experiments focuses on summer effects in which subsurface responses are simulated under conditions of warmer summers and increased summer decoupling (see section 5b). Each of the three panels represents a simulated scenario: (top) A—6 yr of warm summers in which the peak SAT increase from the spinup value of 3–3.15 K, (middle) B—6 yr of increased summer decoupling in which the minimum summer coupling coefficient is reduced from the spinup value of 4–3, and (bottom) C—6 yr of warm summers and increased decoupling in which scenarios A and B are combined.

the appendix). The SAT at Cape Hatteras was approximated in the simulation by a least squares regression fit of the SAT data to a sinusoid during the 1997–98 yr, providing a sinusoid with a period of 1 yr to represent the SAT. The same functional form of the coupling coefficient shown in Fig. 1 was used, but the minimum summer and winter values were adjusted to provide the best correspondence with observations. While there are notable differences between observations and simulations, particularly in the first several tens of centimeters beneath the surface, these differences are reduced after the first meter or two. The principal conclusion to be drawn from Fig. 12 is that below the first meter, where the high frequencies have been sufficiently attenuated, the simulation is remarkably similar to subsurface observations. This is surprising given the relatively simple representations of the SAT and coupling coefficient functions. This suggests that SLIM can capture the gross characteristics of land-atmosphere coupling and the subsequent evolution of subsurface temperatures, even if some of the near-surface details are missed.

While the corroborating evidence presented lends

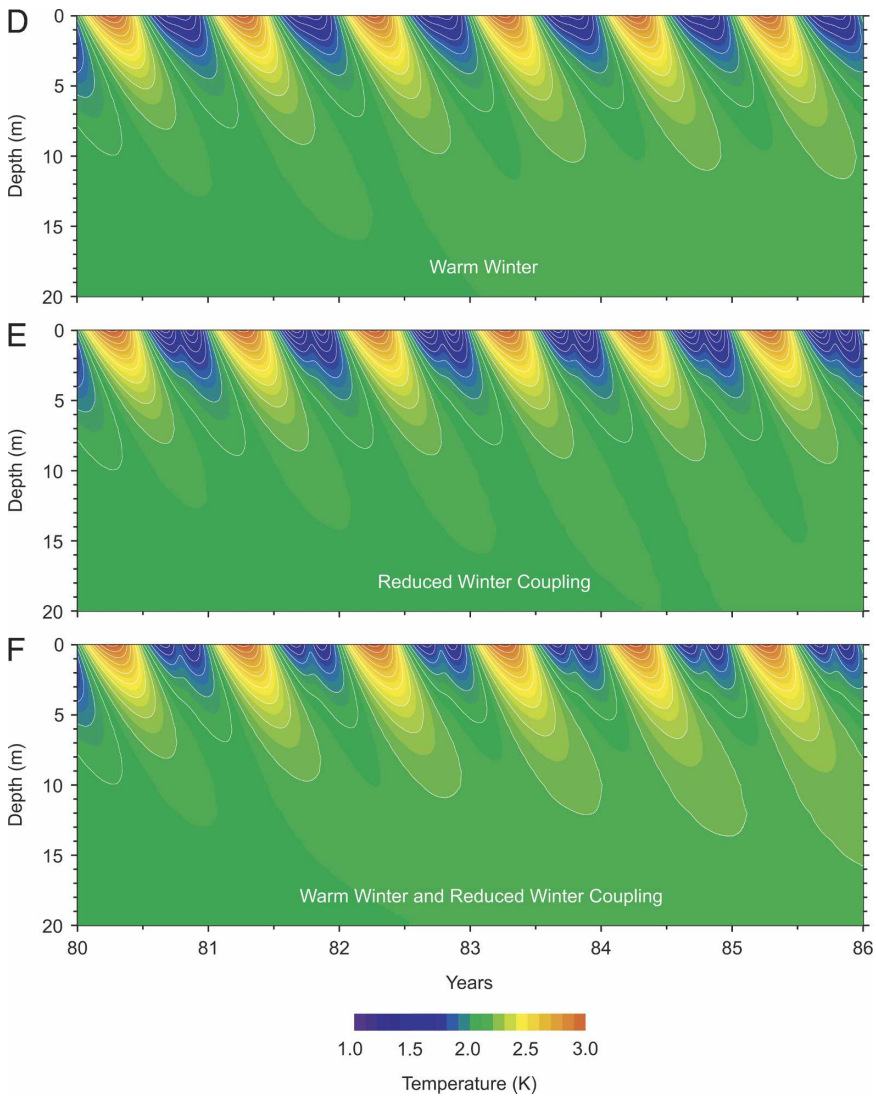

FIG. 9. Results from 6 yr of simulation after perturbations were imposed from the spinup conditions. This ensemble of experiments focuses on winter effects in which subsurface responses are simulated under conditions of warmer winters and reduced winter coupling (see section 5c). Each of the three panels represents a simulated scenario: (top) D—6 yr of warm winters in which the minimum winter temperature increases from the spinup value of 1–1.3 K, (middle) E—6 yr of reduced winter coupling in which the minimum winter coupling coefficient is reduced from the spinup value of 1–0, and (bottom) F—6 yr of warm winters and reduced winter coupling in which scenarios D and E are combined.

credence to the use of SLIM to understand basic land–atmosphere coupling and the subsequent implications for subsurface thermodynamics, there are caveats to consider. The first of which relates to the simple functional forms of SAT and $c(t)$ that we have employed. Further investigations into how these two functions are represented in SLIM, particularly the character and time evolution of the coupling coefficient, will help refine the applicability of SLIM in subsequent investigations. We also note that we have not incorporated latent heat effects in this version of SLIM. The impact of latent heat effects can be implicitly accounted for by incorporating a time- and space-dependent thermal diffusivity in the one-dimensional diffusion equation. A similar approach has been validated at Fargo where subsurface temperature also experience freeze–thaw cycles (Pollack et al. 2005). Preliminary investigations into this representation of subsurface cryogenic pro-

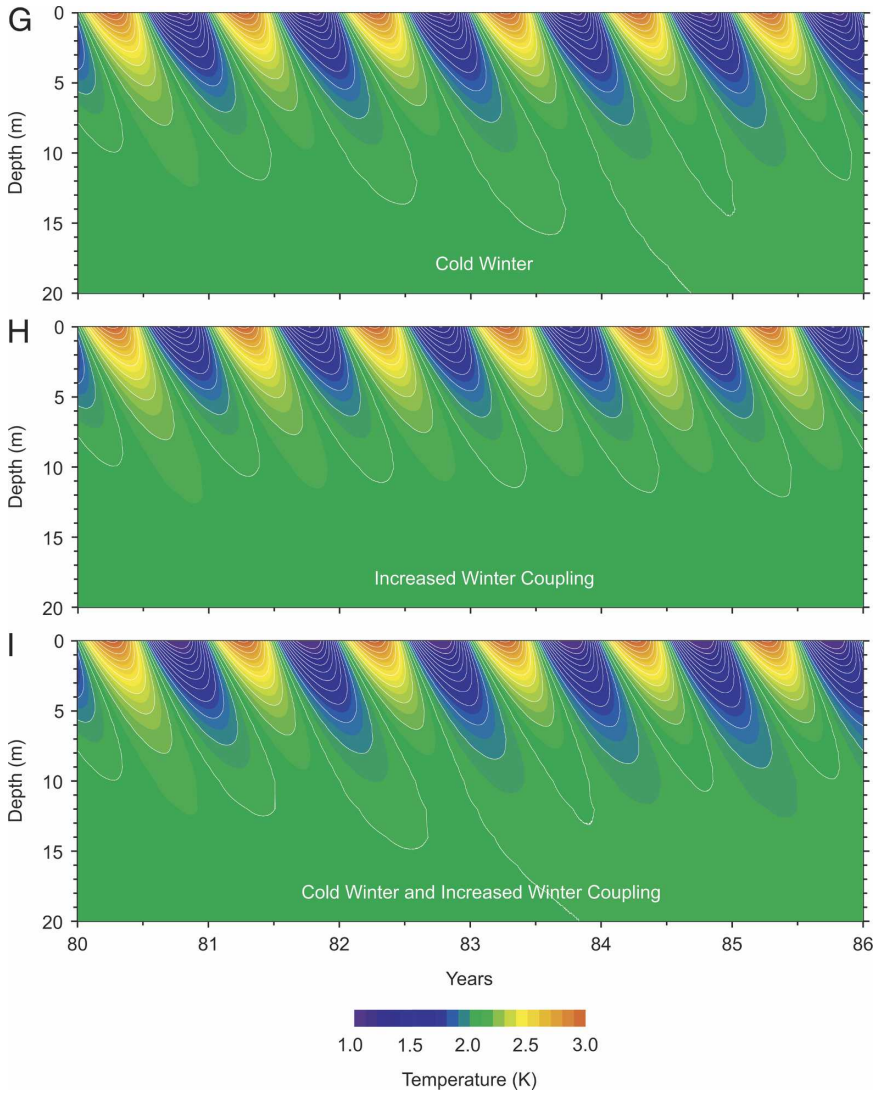

FIG. 10. Results from 6 yr of simulation after perturbations were imposed from the spinup conditions. This ensemble of experiments focuses on winter effects in which subsurface responses are simulated under conditions of colder winters and increased winter coupling (see section 5d). Each of the three panels represents a simulated scenario: (top) G—6 yr of cold winters in which the minimum winter temperature decreases from the spinup value of 1–0.7 K, (middle) H—6 yr of increased winter coupling in which the minimum winter coupling coefficient is increased from the spinup value of 1–3, and (bottom) I—6 yr of cold winters and increased winter coupling in which the changes from scenarios G and H are combined.

cesses have demonstrated the ability of SLIM to approximate freeze–thaw dynamics; this is the subject of ongoing work.

6. Conclusions

The objective of this study was to arrive at a qualitative understanding of land–atmosphere dynamics and the subsequent controls on the seasonal evolution of subsurface temperatures. What separates this modeling exercise from complex modeling studies is that we do not explicitly model the details of the full energy balance at the land surface. We have used an implicit representation of the processes active at the land–atmosphere boundary by assuming a temporally varying SAT and coupling coefficient. Our approach yields qualitative insight into how changing land–atmosphere dynamics impact subsurface thermodynamics over sev-

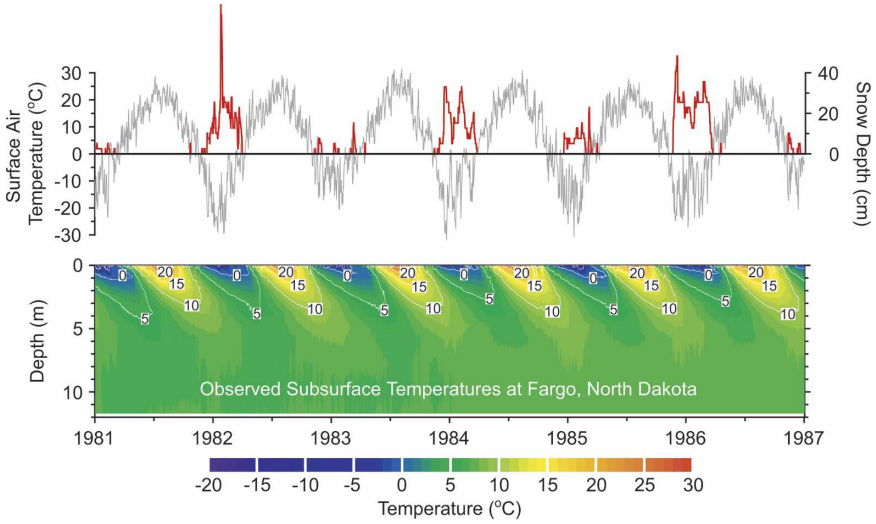

FIG. 11. Observations of (top) meteorological conditions and (bottom) subsurface temperatures down to a depth of 11.7 m at Fargo, ND, from 1 Jan 1981 to 31 Dec 1986. (top) SATs (gray) and snow cover (red) during the period of observation. The ordinate scaling is the same as the simulated temperatures in Figs. 7–9.

eral years, and demonstrate the usefulness of simple modeling frameworks.

The principal utility of the simulations in section 5 are the straightforward insights they provide into the seasonal thermodynamics of the subsurface. We summarize the most important conclusions derived from these simulations as follows:

- The evolution of subsurface thermodynamics on seasonal time scales can be influenced by temperatures at depths as deep as 5–10 m. The importance of these depths in near-surface temperature evolution should not be overlooked in observational and modeling studies.
- The seasonal thermal memory of the subsurface plays

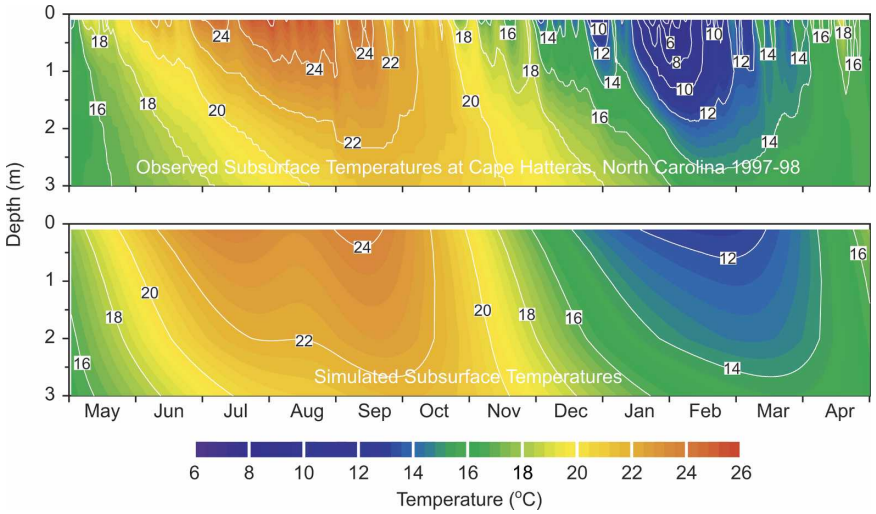

FIG. 12. (top) Observed and (bottom) simulated temperatures at Cape Hatteras, NC, from 1 May 1997 to 30 Apr 1998. SLIM simulations do not capture many of the details of the near-surface temperature evolution, but match much of the deeper signal in the observations. Measurements only extend to 3 m, and therefore the ordinate scaling is expanded, relative to the other contour plots in the paper, to provide more detail.

an important role in the evolution of subsurface temperatures on intraseasonal time scales.
- Reduced summer coupling has the potential to cause colder winter ground temperatures. This effect is the result of reduced summer heat stored in the subsurface, which in turn allows cold winter temperatures to penetrate more deeply.
- Reduced winter coupling increases the relevance of previous seasonal effects. This is most notably displayed in Fig. 9 in which double-bulge features demonstrate the tendency for early winter temperatures to be more strongly affected than temperatures later in the winter if the subsurface is significantly decoupled from SAT. This effect may explain the apparent paradox in the Arctic growing seasons that have expanded in both spring and fall, while the majority of warming has occurred in winter and spring.
- Simple models can capture some of the basic dynamics of the land surface system and are useful for understanding its net effects on subsurface temperature evolution.

Each of the above listed conclusions requires further investigations, but SLIM has provided early evidence for their importance in evolving subsurface temperatures. In this sense, SLIM may work most effectively as a hypothesis generator, the postulates of which can be investigated with observations and further modeling studies. Thus, simple models allow one to better understand land–atmosphere coupling and subsurface thermodynamics from a qualitative point of view, while complex models can be used for prediction and hypothesis testing. It is our contention that when used in tandem, simple and complex models will lead to deeper insights into the fundamental dynamics of land–atmosphere dynamics and subsurface thermodynamics in natural systems.

Acknowledgments. We thank Dr. John Enz at the North Dakota State University and Dr. John Wehmiller at the University of Delaware for providing the observational data from Fargo and Cape Hatteras; both researchers have been very generous with their data and insight. This research was supported in part by NSF grants from the Office of Polar Programs (OPP-002369), the division of Environmental Biology (Arctic LTER Project), NSF Biocomplexity Award ATM 0221835, as well as by the NASA Seasonal-to-Interannual Prediction Project at Goddard Space Flight Center, NASA's Global Modeling and Analysis Program RTOP 622-24-47. Smerdon was additionally supported by a Lamont-Doherty Postdoctoral Fellowship from the Lamont-Doherty Earth Observatory of Columbia University.

APPENDIX

Characterizing Annual SAT and GST Signals

The empirical analysis that we perform is described in detail by Smerdon et al. (2003). The general approach is as follows: 1) extract the annual Fourier component from SAT and each subsurface temperature time series, 2) extrapolate the amplitudes and phases of subsurface Fourier components to the ground surface to estimate an annual GST signal, and 3) compare the annual SAT and GST signals to derive percent attenuation estimates in the summer and winter seasons.

Smerdon et al. (2004) analyzed data from Fargo, Cape Hatteras, and Cape Henlopen to estimate the percent differences between amplitudes in annual GST and SAT signals. Fargo is a grassland site and is representative of a midlatitude intercontinental climate. Based on meteorological station data from the nearby Fargo airport, the site experiences modest rain-equivalent precipitation (54 cm yr^{-1}, estimated in the period 1981–99), significant annual snowfall (123 cm yr^{-1}, in the period 1981–99), and annual snow cover days (96 days yr^{-1}, in the period 1981–95). Cape Henlopen and Cape Hatteras are maritime sites located on partially shaded grassy dunes. Nearby meteorological stations measured more than twice the amount of mean annual rain-equivalent precipitation than Fargo (~110 cm yr^{-1} at each site measured in the period 1996–2001) and both sites experience little or no snow. The amplitudes of annual GST signals were attenuated by 22.5%, 8.3% and 7.6% at Fargo, Cape Henlopen, and Cape Hatteras, respectively, most of which occurred in the winter at Fargo and in the summer at the two capes (see Smerdon et al. 2004, their Fig. 3).

Using the Ameriflux database, we have analyzed annual SATs and GSTs from three sites: Campbell River, Sylvania Wilderness, and Bondville. The Campbell River site is classified as a needle leaf boreal forest located in a 50-yr-old costal Douglas fir stand on the east coast of Vancouver Island (for a detailed description of the site see Humphreys et al. 2003). Thirty-year (1971–2000) normals of mean annual air temperature and annual rain-equivalent precipitation measured at the nearby Campbell River Airport meteorological station (49°57′N, 125°16′W) were 8.6°C and 134.4 cm, respectively, with approximately 109 cm of annual snowfall (more information available online at http://www.ec.gc.ca/envhome.html). The Sylvania Wilderness site is classified as a mixed forest that comprises a canopy of sugar maple, with smaller representations of hemlock, yellow birch, basswood, and ironwood (for a detailed description of the site see Desai et al. 2005).

Thirty-year (1971–2000) normals of mean annual air temperature and annual rain-equivalent precipitation measured at the nearby Watersmeet meteorological station (46°17′N, 89°17′W) were 3.9°C and 77.1 cm, respectively (Desai et al. 2005). The total annual snowfall in the Sylvania Wilderness region averages more than 400 cm (Bockheim and Jordan 2004). The Bondville site is classified as a cropland site where the yearly crop alternates between maize and soybeans (for a detailed description of the site see Meyers and Hollinger 2004). Thirty-year (1971–2000) normals of mean annual air temperature and annual rain-equivalent precipitation measured at the nearby Urbana meteorological station (40°05′N, 88°13′W) were 10.9°C and 104.3 cm, respectively, with approximately 66.5 cm of annual snowfall. Analyses of 1 yr of data from each of these three sites yield the annual signals shown in Fig. 4 and the range of coupling estimates that are provided in section 3c.

REFERENCES

Baker, J. M., and D. G. Baker, 2002: Long-term ground heat flux and heat storage at a mid-latitude site. *Climatic Change,* **54,** 295–303.

Bartlett, M. G., D. S. Chapman, and R. N. Harris, 2004: Snow and the ground temperature record of climate change. *J. Geophys. Res.,* **109,** F04008, doi:10.1029/2004JF000224.

——, ——, and ——, 2005: Snow effect on North American ground temperatures, 1950–2002. *J. Geophys. Res.,* **110,** F03008, doi:10.1029/2005JF000293.

Beltrami, H., 2001: On the relationship between ground temperature histories and meteorological records: A report on the Pomquet station. *Global Planet. Change,* **29,** 327–348.

——, and L. Kellman, 2003: An examination of short- and long-term air-ground temperature coupling. *Global Planet. Change,* **38,** 291–303.

——, A. M. Jessop, and J. C. Mareschal, 1992: Ground temperature histories in eastern and central Canada from geothermal measurements: Evidence of climatic change. *Palaeogeogr. Palaeoclimatol. Palaeoecol.,* **98,** 167–184.

Betts, A. K., J. H. Ball, A. C. M. Beljaars, M. J. Miller, and P. A. Viterbo, 1996: The land surface–atmosphere interaction: A review based on observations and global modeling perspectives. *J. Geophys. Res.,* **101,** 7209–7225.

Bockheim, J. G., and J. K. Jordan, 2004: Soils of the Sylvania Wilderness-Recreation Area, western Upper Peninsula, Michigan. General Tech. Rep. NC-237, U.S. Department of Agriculture, Forest Service, North Central Research Station, St. Paul, MN, 18 pp.

Bodri, L., and V. Cermak, 1995: Climate changes of the last millennium inferred from borehole temperatures: Results from the Czech Republic—Part I. *Global Planet. Change,* **11,** 111–123.

——, and ——, 1997: Climate changes of the last millennium inferred from borehole temperatures: Results from the Czech Republic—Part II. *Global Planet. Change,* **14,** 163–173.

Campbell, G. S., 1977: *An Introduction to Environmental Biophysics*. Springer-Verlag, 159 pp.

Carslaw, H. S., and J. C. Jaeger, 1959: *Conduction of Heat in Solids.* 2d ed. Oxford University Press, 510 pp.

Chapman, W. L., and J. E. Walsh, 1993: Recent variations of sea ice and air temperature in high latitudes. *Bull. Amer. Meteor. Soc.,* **74,** 33–47.

Chisholm, T., and D. S. Chapman, 1992: Climate change inferred from analysis of borehole temperatures: An example from western Utah. *J. Geophys. Res.,* **97,** 14 155–14 177.

Dai, Y., and Coauthors, 2003: The common land model. *Bull. Amer. Meteor. Soc.,* **84,** 1013–1023.

Desai, A. R., P. V. Bolstad, B. D. Cook, K. J. Davis, and E. V. Carey, 2005: Comparing net ecosystem exchange of carbon dioxide between an old-growth and mature forest in the upper Midwest, USA. *Agric. For. Meteor.,* **128,** 33–55.

Dickenson, R. E., and A. Henderson-Sellers, 1988: Modeling tropical deforestation—A study of GCM land surface parameterizations. *Quart. J. Roy. Meteor. Soc.,* **114,** 439–462.

Foster, J. L., 1989: The significance of the date of snow disappearance on the Arctic tundra as a possible indicator of climate change. *Arct. Alp. Res.,* **21,** 60–70.

——, J. W. Winchester, and E. G. Dutton, 1992: The date of snow disappearance on the Arctic tundra as determined from satellite, meteorological station and radiometric in situ observations. *IEEE Trans. Geosci. Remote Sens.,* **30,** 793–798.

Garratt, J. R., 1993: Sensitivity of climate simulations to land-surface and atmospheric boundary-layer treatments—A review. *J. Climate,* **6,** 419–449.

Geiger, R., R. H. Aron, and P. Todhunter, 2003: *The Climate near the Ground*. Rowman & Littlefield, 684 pp.

Gildyal, B. P., and R. P. Tripathi, 1987: *Soil Physics*. Wiley Eastern Ltd., 656 pp.

Goodrich, L. E., 1982: The influence of snow cover on the ground thermal regime. *Can. Geotech. J.,* **19,** 421–432.

Gosnold, W. D., P. E. Todhunter, and W. Schmidt, 1997: The borehole temperature record of climate warming in the mid-continent of North America. *Global Planet. Change,* **15,** 33–45.

Grundstein, A., P. Todhunter, and T. Mote, 2005: Snow pack control over the thermal offset of air and soil temperatures in eastern North Dakota. *Geophys. Res. Lett.,* **32,** L08503, doi:10.1029/2005GL022532.

Harris, R. N., and W. D. Gosnold, 1999: Comparisons of borehole temperature-depth profiles and surface air temperatures in the northern plains of the USA. *Geophys. J. Int.,* **138,** 541–548.

——, and D. S. Chapman, 2001: Mid-latitude (30°–60°) climatic warming inferred by combining borehole temperatures with surface air temperatures. *Geophys. Res. Lett.,* **28,** 747–750.

Henderson-Sellers, A., Z.-L. Yang, and R. E. Dickinson, 1993: The Project for Intercomparison of Land-surface Parameterization Schemes. *Bull. Amer. Meteor. Soc.,* **74,** 1335–1349.

——, A. J. Pitman, P. K. Love, P. Irannejad, and T. H. Chen, 1995: The Project for Intercomparison of Land surface Parameterization Schemes (PILPS): Phases 2 and 3. *Bull. Amer. Meteor. Soc.,* **76,** 489–503.

Hillel, D., 1998: *Environmental Soil Physics*. Academic Press, 771 pp.

Houghton, J. T., Y. Ding, D. J. Griggs, M. Noguer, P. J. van der Linden, X. Dai, K. Maskell, and C. A. Johnson, Eds., 2001: *Climate Change 2001: The Scientific Basis*. Cambridge University Press, 944 pp.

Hu, Q., and S. Feng, 2005: How have soil temperatures been affected by the surface temperature and precipitation in the

Eurasian continent? *Geophys. Res. Lett.,* **32,** L14711, doi:10.1029/2005GL023469.

Huang, S., H. N. Pollack, and P. Y. Shen, 2000: Temperature trends over the last five centuries reconstructed from borehole temperatures. *Nature,* **403,** 756–758.

Humphreys, E. R., T. A. Black, G. J. Ethier, G. B. Drewitt, D. L. Spittlehouse, E.-M. Jork, Z. Nesic, and N. J. Livingston, 2003: Annual and seasonal variability of sensible and latent heat fluxes above a coastal Douglas-fir forest, British Columbia, Canada. *Agric. For. Meteor.,* **115,** 109–125.

Kane, D. L., K. M. Hinkel, D. J. Goering, L. D. Hinzman, and S. I. Outcalt, 2001: Non-conductive heat transfer associated with frozen soils. *Global Planet. Change,* **29,** 275–292.

Karl, T. R., C. N. Williams Jr., F. T. Quinlan, and T. A. Boden, 1990: United States Historical Climatology Network (HCN) serial temperature and precipitation data. Environmental Science Division, Publ. 3404, Carbon Dioxide Information and Analysis Center, Oak Ridge National Laboratory, Oak Ridge, TN, 389 pp.

Koster, R. D., and M. J. Suarez, 1992: Modeling the land surface boundary in climate models as a composite of independent vegetation stands. *J. Geophys. Res.,* **97,** 2697–2715.

——, ——, A. Ducharne, M. Stieglitz, and P. Kumar, 2000: A catchment-based approach to modeling land surface processes in a GCM. Part I: Model structure. *J. Geophys. Res.,* **105,** 24 809–24 822.

Lachenbruch, A. H., and B. V. Marshall, 1986: Changing climate: Geothermal evidence from permafrost in the Alaskan Arctic. *Science,* **234,** 689–696.

Lin, X., J. E. Smerdon, A. W. England, and H. N. Pollack, 2003: A model study of the effects of climatic precipitation changes on ground temperatures. *J. Geophys. Res.,* **108,** 4230, doi:10.1029/2002JD002878.

McBean, G., and Coauthors, 2005: Arctic climate—Past and present. *Arctic Climate Impact Assessment,* C. Symon, L. Arris, and B. Heal, Eds., Cambridge University Press, 22–55.

Meyers, T. P., and S. E. Hollinger, 2004: An assessment of storage terms in the surface energy balance of maize and soybean. *Agric. For. Meteor.,* **125,** 105–115.

Oberman, N. F., and G. G. Mazhitova, 2001: Permafrost dynamics in the North-East of European Russia at the end of the 20th century. *Norwegian J. Geogr.,* **55,** 241–244.

Osterkamp, T. E., and V. E. Romanovsky, 1994: Characteristics of changing permafrost temperatures in the Alaskan arctic, USA. *Arct. Alp. Res.,* **28,** 267–273.

——, and ——, 1999: Evidence for warming and thawing of discontinuous permafrost in Alaska. *Permafrost Periglacial Process.,* **10,** 17–37.

Overpeck, J., and Coauthors, 1997: Arctic environmental change of the last four centuries. *Science,* **278,** 1251–1256.

Pavlov, A. V., 1994: Current changes of climate and permafrost in the Arctic and Sub-Arctic of Russia. *Permafrost Periglacial Process.,* **5,** 101–110.

Pitman, A. J., 2003: The evolution of, and revolution in, land surface schemes designed for climate models. *Int. J. Climatol.,* **23,** 479–510.

Pollack, H. N., and J. E. Smerdon, 2004: Borehole climate reconstructions: Spatial structure and hemispheric averages. *J. Geophys. Res.,* **109,** D11106, doi:10.1029/2003JD004163.

——, D. Y. Demezhko, A. D. Duchkov, I. V. Golovanova, S. Huang, V. A. Shchapov, and J. E. Smerdon, 2003: Surface temperature trends in Russia over the past five centuries reconstructed from borehole temperatures. *J. Geophys. Res.,* **108,** 2180, doi:10.1029/2002JB002154.

——, J. E. Smerdon, and P. E. van Keken, 2005: Variable seasonal coupling between air and ground temperatures: A simple representation in terms of subsurface thermal diffusivity. *Geophys. Res. Lett.,* **32,** L15405, doi:10.1029/2005GL023869.

Putnam, S. N., and D. S. Chapman, 1996: A geothermal climate change observatory: First year results from Emigrant Pass in northwest Utah. *J. Geophys. Res.,* **101,** 21 877–21 890.

Roy, S., R. N. Harris, R. U. M. Rao, and D. S. Chapman, 2002: Climate change in India inferred from geothermal observations. *J. Geophys. Res.,* **107,** 2138, doi:10.1029/2001JB000536.

Schmidt, W. L., W. D. Gosnold, and J. W. Enz, 2001: A decade of air-ground temperature exchange from Fargo, North Dakota. *Global Planet. Change,* **29,** 311–325.

Sellers, P. J., and Coauthors, 1997: Modeling the exchanges of energy, water, and carbon between continents and the atmosphere. *Science,* **275,** 502–509.

Serreze, M. C., and Coauthors, 2000: Observational evidence of recent change in the northern high-latitude environment. *Climatic Change,* **46,** 159–207.

Smith, N. V., S. S. Saatchi, and J. T. Randerson, 2004: Trends in high northern latitude soil freeze and thaw cycles from 1988 to 2002. *J. Geophys. Res.,* **109,** D12101, doi:10.1029/2003JD004472.

Smerdon, J. E., H. N. Pollack, J. W. Enz, and M. J. Lewis, 2003: Conduction-dominated heat transport of the annual temperature signal in soil. *J. Geophys. Res.,* **108,** 2431, doi:10.1029/2002JB002351.

——, ——, V. Cermak, J. W. Enz, M. Kresl, J. Safanda, and J. F. Wehmiller, 2004: Air-ground temperature coupling and subsurface propagation of annual temperature signals. *J. Geophys. Res.,* **109,** D21107, doi:10.1029/2004JD005056.

——, ——, ——, ——, ——, ——, and ——, 2006: Daily, seasonal and annual relationships between air and subsurface temperatures. *J. Geophys. Res.,* **111,** D07101, doi:10.1029/2004JD005578.

Sokratov, S. A., and R. G. Barry, 2002: Intraseasonal variation in the thermoinsulation effect of snow cover on soil temperature and energy balance. *J. Geophys. Res.,* **107,** 4093, doi:10.1029/2001JD000489.

Stieglitz, M., D. Rind, J. Famiglietti, and C. Rosenzweig, 1997: An efficient approach to modeling the topographic control of surface hydrology for regional and global climate modeling. *J. Climate,* **10,** 118–137.

——, A. Ducharne, R. D. Koster, and M. J. Suarez, 2001: The impact of detailed snow physics on the simulation of snow-cover and subsurface thermodynamics at continental scales. *J. Hydrometeor.,* **2,** 228–242.

——, S. J. Dery, V. E. Romanovsky, and T. E. Osterkamp, 2003: The role of snow cover in the warming of arctic permafrost. *Geophys. Res. Lett.,* **30,** 1721, doi:10.1029/2003GL017337.

Stone, R. S., E. G. Dutton, J. M. Harris, and D. Longenecker, 2002: Earlier spring snowmelt in northern Alaska as an indicator of climate change. *J. Geophys. Res.,* **107,** 4089, doi:10.1029/2000JD000286.

Zhang, T., T. E. Osterkamp, and K. Stamnes, 1997: Effects of climate on active layer and permafrost on the North Slope of Alaska. *Permafrost Periglacial Process.,* **8,** 45–67.

——, R. G. Barry, D. Gilichinsky, S. S. Bykhovets, V. A. Sorokovikov, and J. Ye, 2001: An amplified signal of climatic change in soil temperatures during the last century at Irkutsk, Russia. *Climatic Change,* **49,** 41–76.